PHYSICAL REVIEW C, VOLUME 61, 034318

Shears mechanism in ^{109}Cd

C. J. Chiara,[1] S. J. Asztalos,[2] B. Busse,[2] R. M. Clark,[2] M. Cromaz,[2] M. A. Deleplanque,[2] R. M. Diamond,[2] P. Fallon,[2] D. B. Fossan,[1] D. G. Jenkins,[3] S. Juutinen,[4] N. S. Kelsall,[3] R. Krücken,[2,*] G. J. Lane,[1,†] I. Y. Lee,[2] A. O. Macchiavelli,[2] R. W. MacLeod,[2] G. Schmid,[2] J. M. Sears,[1] J. F. Smith,[1,‡] F. S. Stephens,[2] K. Vetter,[2] R. Wadsworth,[3] and S. Frauendorf[5,§]

[1]*Department of Physics and Astronomy, State University of New York at Stony Brook, Stony Brook, New York 11794-3800*
[2]*Nuclear Science Division, Lawrence Berkeley National Laboratory, Berkeley, California 94720*
[3]*Department of Physics, University of York, Heslington, York, YO1 5DD, United Kingdom*
[4]*Department of Physics, University of Jyväskylä, P.O. Box 35, FIN-40351 Jyväskylä, Finland*
[5]*Department of Physics, University of Notre Dame, Notre Dame, Indiana 46556*

(Received 11 October 1999; published 23 February 2000)

Lifetimes of high-spin states in two $\Delta I=1$ bands and one $\Delta I=2$ band in ^{109}Cd have been measured using the Doppler shift attenuation method in an experiment performed using the ^{96}Zr(^{18}O,5n) reaction with the GAMMASPHERE array. Experimental total angular momenta and reduced transition strengths for both $\Delta I=1$ bands were compared with tilted axis cranking (shears mechanism) predictions and the $\Delta I=2$ band with principal axis cranking predictions, based on configurations involving two proton $g_{9/2}$ holes and one or three valence quasineutrons from the $h_{11/2}$ and mixed $g_{7/2}/d_{5/2}$ orbitals. Good overall agreement for angular momentum versus rotational frequency has been observed in each case. The $\Delta I=2$ band is shown to have a large $\mathcal{J}^{(2)}/B(E2)$ ratio suggestive of antimagnetic rotation. Additionally, both dipole bands show a decreasing trend in $B(M1)$ strength as a function of spin, a feature of the shears mechanism. The experimental results are also compared with a semiclassical model that employs effective interactions between the proton holes and neutrons as an alternate interpretation for the shears mechanism.

PACS number(s): 21.10.Tg, 27.60.+j, 23.20.Lv

I. INTRODUCTION

In a number of recent studies, sequences of magnetic dipole transitions that exhibit energy spectra characteristic of collective rotational bands have been observed near the $Z=82$ [1–3] and $Z=50$ closed shells [4–7]. Generally, however, the associated band structures have weak or unobserved $E2$ crossover transitions, suggesting that they arise from a mechanism other than collective rotation. The shears mechanism, a prediction of the tilted axis cranking (TAC) theory [8], describes a process by which a nearly spherical nucleus can generate angular momentum in a manner that resembles rotational motion.

Nuclei in the $A\approx 110$ region with $Z\approx 50$ have low-lying states containing one or more proton holes in the high-Ω $g_{9/2}$ orbitals, and neutrons in the low-Ω $g_{7/2}/d_{5/2}$ and $h_{11/2}$ orbitals. At the bandhead, the proton ($\mathbf{j}_\pi$) and neutron ($\mathbf{j}_\nu$) spin vectors are approximately perpendicular to each other, summing to the total angular momentum $\mathbf{J}$, as shown schematically in Fig. 1(a). The nucleus generates angular momentum by gradually aligning the individual spin vectors (the ‘‘blades’’ of the shears) along the direction of $\mathbf{J}$, which is tilted by the angle θ with respect to the symmetry axis of the nucleus. The magnitude of $\mathbf{J}$ increases as the blades close, with θ remaining nearly constant for a given configuration. An important consequence of this model is that the component of the magnetic dipole vector perpendicular to $\mathbf{J}$, $\mu_\perp$, is large at the bandhead, but decreases as the spin vectors align. This large magnetic dipole vector breaks the intrinsic symmetry of the nucleus and rotates about $\mathbf{J}$, the tilted cranking axis. $\Delta I=1$ bands based on this mechanism are often referred to as magnetic rotational (MR) bands to distinguish them from the cases of collective (electric) rotational bands (see Ref. [9] for a more detailed discussion). The reduced magnetic dipole transition strength $B(M1)$ is proportional to $\mu_\perp^2$; therefore, a distinguishing feature of a MR shears band is a decrease in $B(M1)$ strength with increasing spin. In contrast, bands that approximately maintain a fixed projection K of the angular momentum on the symmetry axis of the nucleus, and generate angular momentum by collective rotation and aligning particle spins along an axis perpendicular to the symmetry axis, have $B(M1)$ values which decrease much less, or even increase, with spin [10]. Lifetime measurements in $^{193-199}$Pb [11–13], ^{108}Cd [14], ^{110}Cd [4], and ^{106,108}Sn [15] have confirmed this feature of shears bands near both the $Z=82$ and $Z=50$ closed shells.

In addition to $\Delta I=1$ shears bands, the possibility of $\Delta I=2$ shears bands, antimagnetic rotation (AMR), is also predicted (see the discussion in Ref. [9]). This mode of excitation is illustrated in Fig. 1(b), where a pair of proton holes are antiparallel at the bandhead, but gradually align along the axis $\mathbf{J}$. Angular momentum can again be generated by the shears mechanism recoupling the proton hole spins, producing a regular sequence of γ-ray transitions without the need

---

[*] Present address: Wright Nuclear Structure Laboratory, Physics Department, Yale University, P.O. Box 208124, New Haven, CT 06520.

[†] Present address: Lawrence Berkeley National Laboratory, Berkeley, CA 94720.

[‡] Present address: Schuster Laboratory, The University of Manchester, Manchester, M13 9PL, United Kingdom.

[§] On leave of absence from Institut für Kern- und Hadronenphysik, Forschungszentrum Rossendorf, PF 510119, D–01314 Dresden, Germany.

0556-2813/2000/61(3)/034318(11)/$15.00

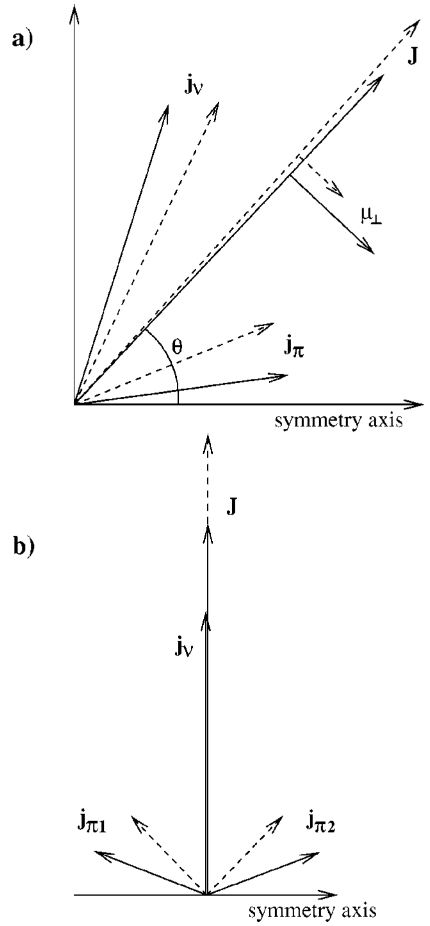

FIG. 1. (a) Illustration of the shears mechanism for a $\Delta I=1$ shears band (magnetic rotation). The spin contribution from the proton holes, $\mathbf{j}_\pi$, and neutron particles, $\mathbf{j}_\nu$, and their corresponding vector sums $\mathbf{J}$, are shown for the $\pi[(g_{9/2})^{-2}]_{8+}\otimes\nu[(g_{7/2}/d_{5/2})\times(h_{11/2})^2]$ configuration, discussed in Sec. IV B. Also shown are the components of the magnetic dipole moment perpendicular to $\mathbf{J}$ at low and high frequencies. Solid and dashed lines are for rotational frequencies $\hbar\omega=0.15$ and 0.55 MeV, respectively. (b) Illustration of the shears mechanism for a $\Delta I=2$ shears band (antimagnetic rotation). The spin contributions from the two proton holes ($\mathbf{j}_{\pi1,2}$) are shown separately. Solid and dashed lines are for rotational frequencies $\hbar\omega=0.40$ and 0.80 MeV, respectively, for the $\pi[(g_{9/2})^{-2}]_{0+}\otimes\nu[(h_{11/2})^3]$ configuration, discussed in Sec. IV A.

for a substantial deformation of the nuclear core. These bands have small $B(E2)$ strengths, which are associated with small deformations. While the distinguishing characteristics of such a band are not as distinctive as for the MR bands, AMR bands are expected to have large $\mathcal{J}^{(2)}/B(E2)$ ratios $[>100\hbar^2\ \mathrm{MeV}^{-1}(e\,\mathrm{b})^{-2}$, compared to $\sim 10\hbar^2\ \mathrm{MeV}^{-1}(e\,\mathrm{b})^{-2}$ for well-deformed nuclei], corresponding to a large contribution to the moment of inertia by quantal effects, i.e., the closing blades of the shears [9]. So far this second mode of shears excitation has not been conclusively proven to exist, though AMR bands have been predicted for the $Z\approx 50$ mass region [16].

Although not illustrated in Fig. 1, there is also, in general, a component of the total angular momentum attributable to collective rotation of the core ($\mathbf{R}$). For nearly spherical nuclei this component is small relative to the shears component, but as deformation increases, competition is expected between these two modes of angular momentum generation. From studies of shears bands in the Pb region, it has been suggested that the shears mechanism should dominate when $\varepsilon_2 \lesssim 0.12$ [17]. In order to better understand this competition, systematic properties of the shears mechanism should be studied in nuclei ranging from (nearly) spherical shapes, cases of pure shears, to significant deformations, where collective rotation dominates.

The TAC theory predicts, for the neutron-deficient $_{48}$Cd isotopes, that the particular nucleon orbitals near the Fermi surface and the known low deformation of these nuclei should make them good candidates for the shears mechanism [18]. Cd nuclei intrinsically have two proton $g_{9/2}$ holes, which can form the high-Ω blade of a $\Delta I=1$ shears [Fig. 1(a)] or both blades of a $\Delta I=2$ shears [Fig. 1(b)]. The neutron orbitals for $N\approx 60$ are filled up to the low-Ω levels of the high-j $h_{11/2}$ subshell, providing the second blade for the $\Delta I=1$ shears. Candidate MR and AMR shears bands have been previously observed in $^{109}_{48}\mathrm{Cd}_{61}$ [19]. We report here on lifetime measurements for these bands and their interpretation in the context of the shears formalism.

II. EXPERIMENTAL DETAILS

High-spin states in ^{109}Cd were populated using the $^{96}\mathrm{Zr}(^{18}\mathrm{O},5n)$ reaction. A 70-MeV ^{18}O beam, provided by the 88-Inch Cyclotron at Lawrence Berkeley National Laboratory, was incident on a $\simeq 500$-μg/cm^2 ^{96}Zr target (enriched to 86%) backed with $\simeq 10$ mg/cm^2 natural Pb. The choice of backing provided sufficient stopping power to slow down and stop the recoiling nuclei produced in this reaction. This allowed measurement of short ($\lesssim 1$ ps) lifetimes of states using the Doppler shift attenuation method (DSAM) [20]. Emitted γ rays were detected with the GAMMASPHERE array [21], consisting of 99 75%-efficient escape-suppressed Ge detectors. The detectors were arranged in 17 rings of constant angle relative to the beam direction: five detectors at 17.3°, five at 31.7°, five at 37.4°, ten at 50.1°, five at 58.3°, nine at 69.8°, four at 79.2°, three at 80.7°, eight at 90.0°, four at 99.3°, four at 100.8°, eight at 110.2°, five at 121.7°, ten at 129.9°, four at 142.6°, five at 148.3°, and five at 162.7°. A total of 9.95×10^8 coincidence events with fold 4 or higher were collected. In addition, a complementary thin-target experiment was performed with an unbacked $\simeq 500$-μg/cm^2 ^{96}Zr target; a total of 4.97×10^8 coincidence events with fold 4 or higher were collected in this experiment.

III. RESULTS

A. Level scheme

The coincidence data from the thin-target experiment were unfolded into threefold events (triples) and sorted into an E_γ-E_γ-E_γ cube. The RADWARE program LEVIT8R [22] was used to project double-gated background-subtracted coincidence spectra from the cube. The level scheme for ^{109}Cd deduced in this analysis extends the level scheme proposed

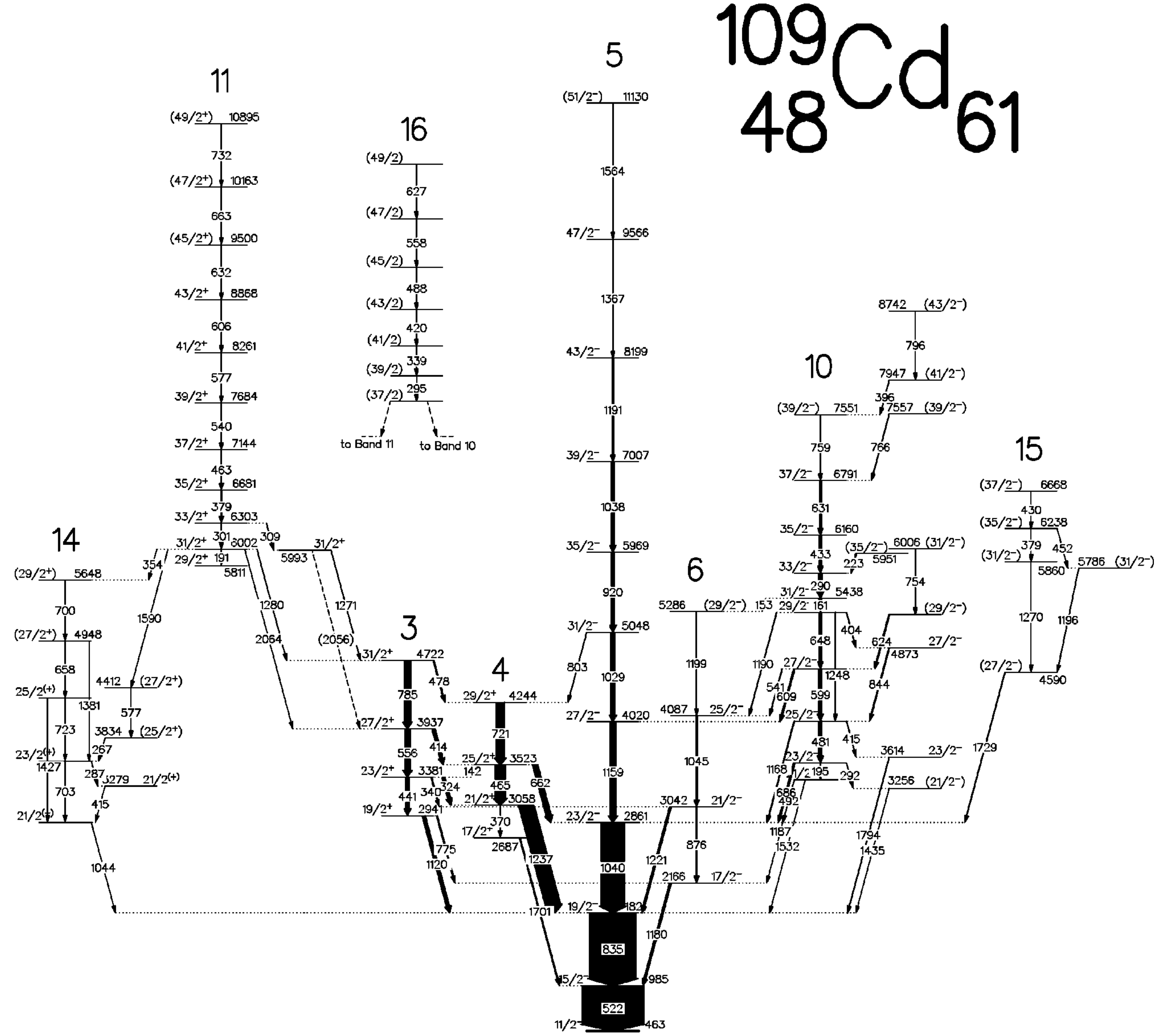

FIG. 2. Partial level scheme of ^{109}Cd. Only those states relevant to the analysis have been included. Widths of arrows are proportional to the fitted intensity of each transition.

by Juutinen *et al.* [19]. The portions of the level scheme relevant to the DSAM analysis are presented in Fig. 2. Those bands which differ significantly from the previous work, namely, bands 11, 14, 15, and 16, are discussed in detail below. A complete level scheme will be reported separately [23]. Throughout the remainder of this discussion and in Fig. 2, the band-labeling scheme used in [19] has been adopted.

Band 14 was shown in the directional correlation (DCO) analysis of Ref. [19] to consist of $\Delta I = 1$ $M1/E2$ transitions with a stretched $E2$ crossover transition. This band has been extended in the current work by the addition of the 658- and 700-keV transitions. In addition, a 1381-keV transition was observed crossing over the 658- and 723-keV transitions. This confirms the ordering of the γ rays and suggests a probable spin of $(\frac{27}{2}^+)$ for the 4948-keV level. Note that band 14 was not included in the DSAM analysis, but has been presented here to identify part of the decay out of band 11, as discussed below.

Band 11 was determined to be a sequence of $\Delta I = 1$ γ rays in Ref. [19]. No crossover transitions were observed. This band was extended to higher spin by three in-band transitions, the 632-, 663-, and 732-keV γ rays. A 191-keV γ ray was also observed feeding out of the bottom of the band. A number of transitions were observed linking band 11 to bands 3 and 14, thus fixing the excitation energies of the members of band 11. These linking transitions were too weak to determine their multipolarities with a DCO analysis. The 1280- and 1271-keV γ rays that connect band 11 to band 3 do feed, however, a state that is $2\hbar$ higher in spin than the state fed by the 2064- and (tentative) 2056-keV γ rays. This suggests that the 1280- and 1271-keV γ rays have $\Delta I = 0$ mixed $M1/E2$ multipolarity, the 2064- and 2056-keV γ rays have stretched $E2$ multipolarity, and, ultimately, the 5993- and 6002-keV levels both have $I^\pi = \frac{31}{2}^+$. Assuming the sequence of $\Delta I = 1$ transitions are of mixed $M1/E2$ character, which is reasonable considering the regularity of the sequence, this fixes the parity of band 11 to be positive. (Additional support for this parity assignment will be provided in Sec. IV B.) The excitation energies of the states in band 11 are further confirmed by the observation of two sequences of γ rays feeding out of the $\frac{31}{2}^+$ state of band 11 into band 14: a 354-keV γ ray feeds directly into the $(\frac{29}{2}^+)$ state of band 14, and a 1590–577–267-keV sequence feeds into the $\frac{23}{2}^{(+)}$ state.

In the previous work [19], band 11 was incorrectly linked to band 5 via a 1271–1729-keV cascade feeding out of the $\frac{33}{2}^+$ state of band 11. In the current analysis, the 1729-keV γ ray was found to be in coincidence with a 1270- and a 379-keV transition, as well as band 5 below $\frac{23}{2}^-$, but not with any other transitions in band 11. Coincidence relationships suggest that there are two 379–1271-keV sequences present in ^{109}Cd, one in band 11 and one in the new structure labeled band 15. This suggestion is supported by the observation of a 452–1196-keV sequence parallel to the 379–1270-keV sequence in band 15. In addition, all members of band 15 are in coincidence with a 430-keV γ ray, which is not in coincidence with band 11.

An additional structure, labeled band 16, was newly observed in this work. This sequence is presumed to be a band of $\Delta I=1$ transitions. No γ rays were found that conclusively linked band 16 with the rest of the level scheme. Furthermore, the intensity of the band was weak, making a meaningful lifetime analysis difficult due to large uncertainties. Band 16 has, therefore, been omitted from the remainder of this discussion.

B. DSAM analysis

The data from the backed-target experiment were unfolded into triples and sorted into angle-dependent gated E_γ-E_γ coincidence matrices. Each matrix included only those events which satisfied the following criteria: (i) at least one γ ray of the triple belonged to a gate list consisting of the 522-, 835-, and 1040-keV transitions at the bottom of band 5 in ^{109}Cd, thus reducing contamination by neighboring nuclei; (ii) at least one of the remaining γ rays in the triple was detected by a Ge detector in a specified ring, and was placed on the *y* axis of the matrix. No restrictions were imposed on the remaining coincident γ ray in the event, which was placed on the *x* (or ‘‘all’’) axis.

Gates were placed on the ‘‘all’’ axis of each matrix at energies corresponding to stopped (or nearly stopped) transitions in each band of interest; the resulting double-gated background-subtracted coincidence spectra for various angles were projected from the matrices. In the cases where the gating transition was not fully stopped, the gate was made wide enough to ensure that the full peak shape was included in the gate; this eliminated a possible DSAM lifetime bias that could be introduced by the omission of the tails of the peak line shape, which contain the fast time component of the gating transition.

Doppler-broadened line shapes were observed for transitions above $I=\frac{27}{2}$ in the $\Delta I=2$ band 5 and above $I=\frac{31}{2}$ in the $\Delta I=1$ bands 10 and 11. For each band, background-subtracted spectra were projected from the matrices corresponding to the rings at angles 17.3°, 31.7°, 37.4°, 50.1°, 90.0°, 129.9°, 142.6°, 148.3°, and 162.7°. Three angle sets were used, each including spectra from forward, transverse, and backward angles. Set *A* consisted of the rings at 17.3°, 90.0°, and 162.7°; set *B* consisted of angles 31.7° and 37.4° (spectra were summed for greater statistics), 90.0°, and 148.3° and 142.6° (summed spectra); set *C* consisted of the rings at 50.1°, 90.0°, and 129.9°. For each angle set, lifetimes of states in the three bands were measured using the LINESHAPE analysis codes of Wells and Johnson [24]. (LINESHAPE permits at most three angles to be fitted at a time.) These codes were used to generate 5000 Monte Carlo simulations of the velocity history of recoiling nuclei traversing the target and backing material in time steps of 0.002 ps. Electronic stopping powers were taken from the tabulations of Northcliffe and Schilling [25], corrected for shell effects. The number of time steps for each history was determined internally by the time required for the kinetic energy of the simulated recoil to decrease to 0.1% of its initial value. Velocity profiles were generated for each (summed) angle based on the detector geometry.

Energies of in-band transitions and side-feeding intensities were extracted from fits to the data in the thin-target cube, and are presented in Table I. These values were used as input parameters for the line shape analysis. Side feeding into each level and feeding into the topmost level of each band was initially modeled as a five-transition cascade with a moment of inertia fixed to be comparable to that of the in-band sequence. The quadrupole moments of the side-feeding sequences were allowed to vary, which, when combined with the moment of inertia, acted as effective side-feeding lifetime parameters for each level.

Starting with the topmost transition in each band, the in-band and side-feeding lifetimes, background parameters, and contaminant-peak parameters were free to vary. For each set of parameters, the simulated line shape was calculated and compared to the corresponding spectrum for each angle using χ^2-minimization routines originating from the program MINUIT [26]. The forward, transverse, and backward spectra for each transition were fitted simultaneously. The best-fit background and stopped contaminant-peak parameters were then fixed, and the in-band and side-feeding lifetimes were used as an effective feeding time parameter for the next level lower in the band. Each level was added and fitted in turn, until the entire band was included in a global fit that had independently variable lifetimes for each in-band and side-feeding level. Examples of the line shape fits for transitions in each band are shown in Fig. 3. Fits for states high in the band were found to be very sensitive to the accuracy with which the side-feeding intensity was known, with the sensitivity decreasing lower in the band. (This was studied by changing the intensity from the measured values in several cases and noting the differences in the fitted lifetimes.) The side-feeding cascades were typically significantly faster than the in-band lifetimes. The side-feeding moment of inertia could be varied considerably and still produce the same lifetime fits, within the quoted errors. Uncertainties in the lifetime measurements were derived from the behavior of the χ^2 fit in the vicinity of the minimum, and include covariance of

TABLE I. Properties of transitions in ^{109}Cd with line shapes which enable DSAM analysis. Transition energies and intensities are from the fits to the thin-target data. The side-feeding intensity into each level, I_{SF}, is the difference between the observed intensity of the in-band transitions feeding out of and into a state. The intensities are relative to $I_\gamma \equiv 100$ for the $I^\pi = \frac{31}{2}^- \rightarrow \frac{27}{2}^-$ 1028.8-keV transition in band 5. Lifetimes τ_i of measured states from each of the three angle sets $i = A, B, C$ are given, as well as the corresponding weighted average $\overline{B(E2)}$ or $\overline{B(M1)}$ reduced transition strengths. Uncertainties in the lifetimes were derived from the covariance of the fitted parameters; systematic uncertainties of up to ±20% are not included. Uncertainties in the transition strengths were calculated from the weighted averages, as described in the text. Also see text for details of the angle sets used in the fits.

E_γ (keV)	$I_i^\pi \rightarrow I_f^\pi$	I_γ	I_{SF}	τ_A (ps)	τ_B (ps)	τ_C (ps)	$\overline{B(E2)}$ $(e\,\mathrm{b})^2$	$\overline{B(M1)}$ (μ_N^2)
				Band 5	$(\Delta I = 2)$			
1028.8	$\frac{31}{2}^- \rightarrow \frac{27}{2}^-$	$\equiv 100$	20.6	$1.22^{+0.10}_{-0.09}$	$1.82^{+0.16}_{-0.12}$	$1.80^{+0.14}_{-0.12}$	$0.043^{+0.005}_{-0.005}$	
920.0	$\frac{35}{2}^- \rightarrow \frac{31}{2}^-$	79.4	10.8	$0.31^{+0.02}_{-0.03}$	$0.40^{+0.03}_{-0.02}$	$0.34^{+0.06}_{-0.01}$	$0.33^{+0.03}_{-0.03}$	
1038.4	$\frac{39}{2}^- \rightarrow \frac{35}{2}^-$	68.6	36.4	$0.41^{+0.05}_{-0.04}$	$0.41^{+0.02}_{-0.01}$	$0.35^{+0.03}_{-0.03}$	$0.166^{+0.004}_{-0.006}$	
1191.2	$\frac{43}{2}^- \rightarrow \frac{39}{2}^-$	32.1	18.5	$0.16^{+0.01}_{-0.02}$	$0.188^{+0.005}_{-0.019}$	$0.192^{+0.008}_{-0.006}$	$0.181^{+0.007}_{-0.006}$	
1366.4	$\frac{47}{2}^- \rightarrow \frac{43}{2}^-$	13.6	10.7	$0.182^{+0.007}_{-0.007}$	$0.172^{+0.009}_{-0.007}$	$0.181^{+0.007}_{-0.009}$	$0.096^{+0.002}_{-0.002}$	
				Band 10	$(\Delta I = 1)$			
289.6	$\frac{33}{2}^- \rightarrow \frac{31}{2}^-$	84.9	33.3	$1.61^{+0.07}_{-0.07}$	$1.38^{+0.04}_{-0.04}$	$1.17^{+0.02}_{-0.11}$		$1.80^{+0.15}_{-0.15}$
432.9	$\frac{35}{2}^- \rightarrow \frac{33}{2}^-$	51.6	10.2	$0.25^{+0.01}_{-0.01}$	$0.264^{+0.007}_{-0.009}$	$0.292^{+0.006}_{-0.008}$		$2.56^{+0.11}_{-0.11}$
631.1	$\frac{37}{2}^- \rightarrow \frac{35}{2}^-$	41.4	25.6	$0.31^{+0.02}_{-0.03}$	$0.28^{+0.01}_{-0.02}$	$0.205^{+0.002}_{-0.007}$		$0.83^{+0.07}_{-0.07}$
759.4	$\frac{39}{2}^- \rightarrow \frac{37}{2}^-$	15.8	9.8	$0.27^{+0.02}_{-0.03}$	$0.34^{+0.02}_{-0.02}$	$0.36^{+0.02}_{-0.03}$		$0.39^{+0.03}_{-0.03}$
				Band 11	$(\Delta I = 1)$			
300.9	$\frac{33}{2}^+ \rightarrow \frac{31}{2}^+$	18.9 [a]	0	$0.41^{+0.04}_{-0.03}$	$0.38^{+0.02}_{-0.02}$	$0.32^{+0.02}_{-0.02}$		$4.45^{+0.29}_{-0.29}$
378.7	$\frac{35}{2}^+ \rightarrow \frac{33}{2}^+$	24.5	3.8	$0.27^{+0.01}_{-0.01}$	$0.250^{+0.008}_{-0.007}$	$0.239^{+0.007}_{-0.014}$		$4.19^{+0.14}_{-0.14}$
462.6	$\frac{37}{2}^+ \rightarrow \frac{35}{2}^+$	20.7	6.4	$0.214^{+0.007}_{-0.009}$	$0.211^{+0.005}_{-0.005}$	$0.204^{+0.005}_{-0.021}$		$2.76^{+0.04}_{-0.04}$
540.1	$\frac{39}{2}^+ \rightarrow \frac{37}{2}^+$	14.3	3.5	$0.097^{+0.006}_{-0.006}$	$0.113^{+0.005}_{-0.010}$	$0.132^{+0.005}_{-0.008}$		$3.15^{+0.32}_{-0.24}$
577.3	$\frac{41}{2}^+ \rightarrow \frac{39}{2}^+$	10.9	1.6	$0.085^{+0.006}_{-0.008}$	$0.071^{+0.006}_{-0.007}$	$0.097^{+0.005}_{-0.013}$		$3.69^{+0.31}_{-0.31}$

[a] The intensity out of the $\frac{33}{2}^+$ state of band 11 is split among the 301-keV, 309-keV, and unobserved transitions. The $B(M1)$ value for the 301-keV γ ray was calculated from its partial lifetime.

the in-band and side-feeding lifetimes. These values are presented in Table I for all three angle sets. Systematic errors associated with the modeling of the stopping powers are not included in the quoted errors, and may be as large as ±20%.

For each band, $B(E2)$ or $B(M1)$ values were calculated from the lifetimes fitted for each angle set using the standard relationships [27]. Effects of internal conversion are negligible in each case. The dipole transitions of bands 10 and 11 were assumed to be of pure magnetic character. No crossover transitions were observed feeding out of any of the fitted levels in either dipole band; the crossover $E2$ component of the intensity of each level was, therefore, set to zero.

The size of the uncertainties, propagated through the calculation of the reduced transition strengths, did not appear to properly reflect the distribution of values measured in the three angle sets. In an effort to better estimate these uncertainties, a χ^2 minimization was performed (fitting a constant value to the three measured points, weighted by their corresponding uncertainties) to find the weighted average for each transition. In most cases, the minimum reduced χ^2, χ^2_ν, was larger than 1.0, sometimes significantly so. Since the function being fitted is of known form (a constant), this suggests that the fitted lifetime uncertainties have been underestimated. To correct this, we have renormalized those uncertainties by the factor $\sqrt{\chi^2_\nu}$; refitting the weighted average results in $\chi^2_\nu \sim 1.0$. The uncertainty in the weighted average was determined as the difference in the value of the average which resulted in a χ^2 increase by 1.0. These weighted averages and uncertainties are also presented in Table I.

IV. DISCUSSION

Self-consistent cranking model calculations were performed for comparison with bands 5, 10, and 11. All calculations were made using TAC codes with the same set of parameters. The $\Delta I = 2$ band 5 involves cranking about a principal axis. For this case we found $\theta = 90°$ by means of the TAC codes, i.e., a principal axis cranking (PAC) solution, which is in accordance with the $\Delta I = 2$ character of the band. For the two $\Delta I = 1$ bands, we found $\theta < 90°$, which is in accordance with their $\Delta I = 1$ character. Proton properties were calculated assuming zero pairing, due to the proximity of the proton Fermi surface to the $Z = 50$ shell gap. The neutron Fermi surface lies sufficiently far from the $N = 50$ closed shell to warrant using a quasiparticle treatment of the neutrons. A neutron-pairing constant of $\Delta_\nu = 1.11$ MeV was determined to be appropriate for ^{109}Cd, calculated as 0.8

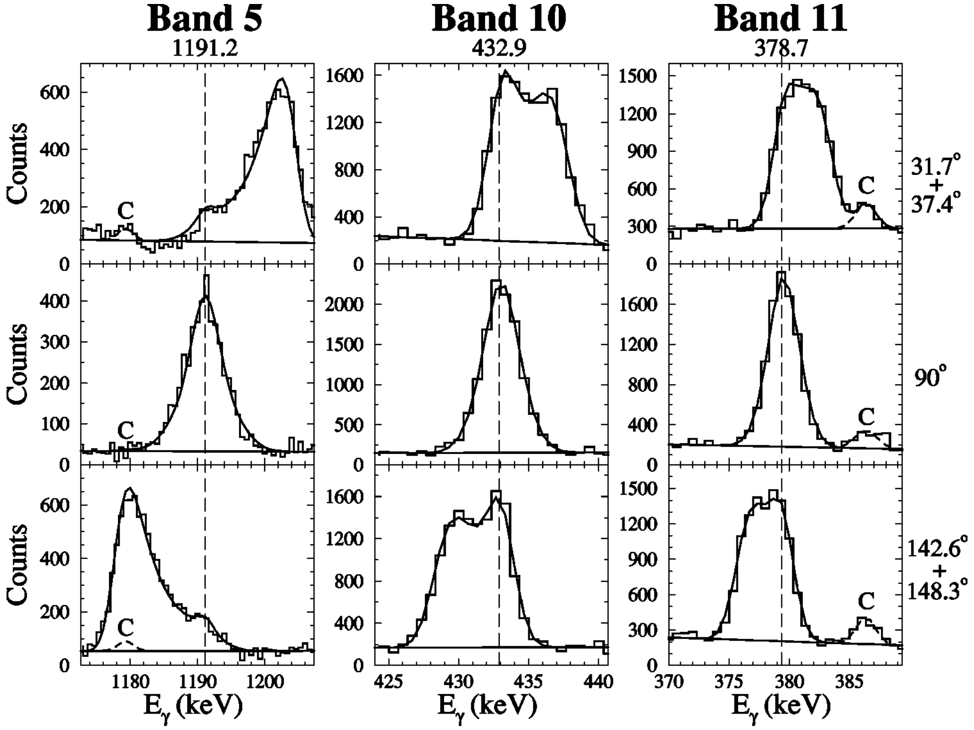

FIG. 3. Experimental data and associated line shape fits for the 1191.2-keV transition in band 5, the 432.9-keV transition in band 10, and the 378.7-keV transition in band 11. The spectra are labeled on the right-hand side with the angles of the rings shown; these fits are for angle set *B*, but are representative of all three angle sets included in the analysis. Contaminant peaks are marked by a ''C.'' The unshifted γ-ray energy for each transition is marked by the vertical dashed line.

times the experimental even-odd mass difference for this nucleus. The neutron chemical potential λ_ν was chosen such that the particle number of $N\approx61$ was reproduced.

A. Band 5

The coupling constant κ for the quadrupole-quadrupole interaction used in these calculations was scaled from Ref. [1] by $A^{-5/3}$. To verify that this scaling was appropriate, κ was also estimated in the following way: PAC calculations were performed for band 5 above the backbend using the configuration $\pi[(g_{9/2})^{-2}]_{0^+}\otimes\nu[(h_{11/2})^3]$. (The configuration assignment for band 5 is discussed in Ref. [19].) The predicted $B(E2)$ values were compared with the weighted averages calculated from the lifetime measurements for this band, and are shown in Fig. 4. The deformation parameter ε_2 was varied until the theory reasonably reproduced the experimental $B(E2)$ strengths. [The perturbed value at $I=\frac{35}{2}$ ($\hbar\omega=0.460$ MeV) will be discussed in Sec. IV B.] κ was then adjusted so that the total energy of the nucleus in the intrinsic frame was minimized for that same value of ε_2. The value obtained with this procedure was $\kappa=0.0355$ MeV/a^2, where $a=1.011A^{1/3}$ fm^2, which is consistent with the value scaled from Ref. [1] and those used in other calculations in this mass region [4,6,7].

The experimental angular momentum as a function of frequency for the $\Delta I=2$ band 5 is compared with corresponding PAC predictions in Fig. 5. Above the backbend, the calculation is for $\nu[(h_{11/2})^3]$ at the equilibrium deformation $\varepsilon_2=0.14$, $\gamma=0°$; at these frequencies, the theoretical predictions are in excellent agreement with the data. A maximum of $8\hbar$ can be generated by fully aligning the proton holes, which, when coupled to three fully aligned $h_{11/2}$ neutrons, yields $I\sim\frac{43}{2}$. The remainder of the spin in band 5 can be attributed to a core rotational component. The contributions to the moment of inertia from the core and the shears are predicted in these calculations to be $\mathcal{J}^{(2)}_{core}=12.8\hbar^2$ MeV^{-1} and $\mathcal{J}^{(2)}_{sh}=15.0\hbar^2$ MeV^{-1}, respectively, where the components of the moment of inertia are defined as the increase in the angular momentum due to the core or the closing shears blades per increase in rotational frequency. Over half the angular momentum is generated by the shears.

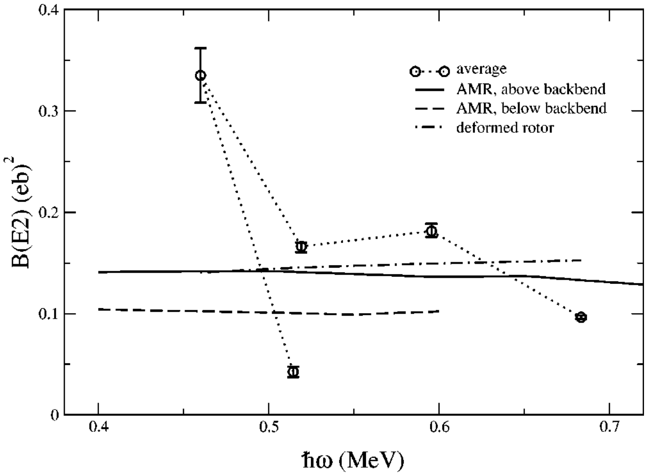

FIG. 4. Reduced $E2$ transition strength $B(E2)$ as a function of frequency for band 5. Experimental values are the weighted averages of all three angle sets, deduced from the fitted lifetimes (see Table I). The dotted line is meant only to indicate the order of the transitions through the backbend. The dashed line shows the PAC prediction for an AMR band with the $\pi[(g_{9/2})^{-2}]_{0^+}\otimes\nu[h_{11/2}]$ configuration, and the solid line is for an AMR band with the $\pi[(g_{9/2})^{-2}]_{0^+}\otimes\nu[(h_{11/2})^3]$ configuration. The dash-dotted line is the TRS prediction for the $B(E2)$ strength of a deformed axial rotor with $\varepsilon_2=0.16$.

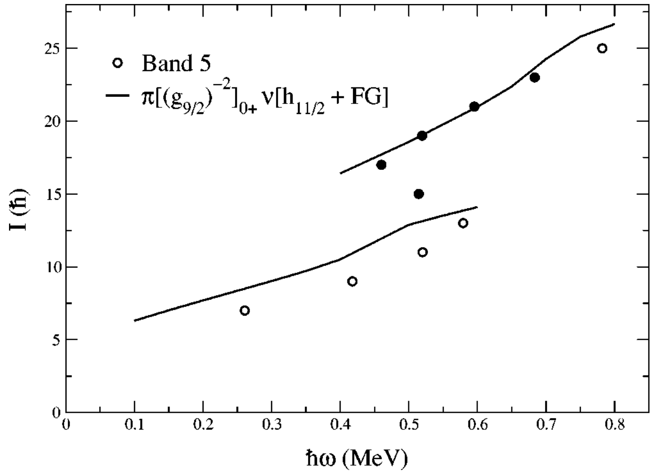

FIG. 5. Angular momentum as a function of frequency for band 5. Solid circles correspond to those transitions for which lifetimes were measured.

Taking the measured $B(E2)$ to be approximately 0.17 $(e\,\mathrm{b})^2$, the $\mathcal{J}^{(2)}_{tot}/B(E2)$ ratio is about $165\hbar^2\ \mathrm{MeV}^{-1}(e\,\mathrm{b})^{-2}$, an order of magnitude larger than expected for a well-deformed rotor. Thus, the band has AMR character, where the angular momentum is generated by the gradual alignment of the two proton spin vectors, as opposed to small contributions of many particles to collective angular momentum of a well-deformed nucleus.

Below, the first allowed $h_{11/2}$ neutron alignment (FG in the standard cranking model convention), the calculation is for $\nu[h_{11/2}]$ at the equilibrium deformation (calculated at $\hbar\omega\approx 0.30$ MeV) of $\varepsilon_2=0.12$, $\gamma=0°$; at these lower frequencies, the theory overestimates the spin by about $2\hbar$. The cranking model used provides a static representation of the valence particles and does not account for fluctuations in the particle spin vectors. The inclusion of a larger number of active particles results in larger vectors, which could reduce the relative size of the fluctuations. This may explain why the calculated $I(\omega)$ improves above the alignment in band 5. For the lower part of the band, $\mathcal{J}^{(2)}_{core}=4.2\hbar^2\ \mathrm{MeV}^{-1}$ and $\mathcal{J}^{(2)}_{sh}=9.8\hbar^2\ \mathrm{MeV}^{-1}$. The lifetimes of transitions below the backbend were not fittable in this analysis, so there are no experimental $B(E2)$ values for comparison. A previous study, however, indicated $B(E2)$ strengths of $\sim 0.1\ (e\,\mathrm{b})^2$ for the 522- and 835-keV transitions [28]. This is consistent with the PAC calculations performed in this analysis, which also predict $B(E2)$ values around 0.1 $(e\,\mathrm{b})^2$ for the lower part of band 5 (see Fig. 4). This results in $\mathcal{J}^{(2)}_{tot}/B(E2)\approx 140\hbar^2\ \mathrm{MeV}^{-1}(e\,\mathrm{b})^{-2}$, again indicating a large quantal contribution to the moment of inertia, and hence AMR character.

The predicted equilibrium deformations are smaller in our PAC calculations than those determined in PAC total Routhian surface (TRS) calculations based on the Woods-Saxon single-particle potential [19]. The latter predict $\varepsilon_2\approx 0.13$ and 0.16 for band 5 below and above the FG alignment, respectively, as compared to our values 0.12 and 0.14, respectively. The $B(E2)$ values obtained by means of TRS calculations with $\varepsilon_2=0.16$ are shown in Fig. 4 for comparison, and are found to be consistent with our values. This implies that the Woods-Saxon potential, which has a different radial form factor than the Nilsson potential we are using, gives a somewhat smaller $B(E2)$ value for the same deformation. A larger fraction of the total angular momentum is generated by the shears in our calculations in comparison with the TRS calculations.

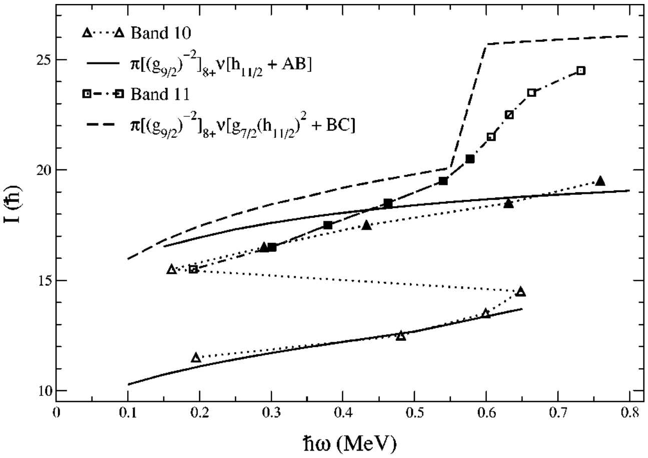

FIG. 6. Angular momentum as a function of frequency for bands 10 and 11. Note that the $g_{7/2}$ label is shorthand for the mixed $g_{7/2}/d_{5/2}$ orbitals. Solid circles correspond to those transitions for which lifetimes were measured.

In both of these PAC calculations, the $B(E2)$ strength is approximately constant. In the case of a pure AMR band (i.e., $\mathbf{R}\equiv 0$), the quadrupole moment of the nucleus would depend solely on the orientation of the active particles. As the particles align, the charge distributions become symmetric about the cranking axis, resulting in $B(E2)$ values that would be expected to decrease to zero as spin increases. The presence of core contributions, providing a nearly constant component to the $B(E2)$ values, makes this behavior difficult to identify. On the basis of the magnitude of the $\mathcal{J}^{(2)}_{tot}/B(E2)$ ratio relative to that of a well-deformed rotor, however, this analysis indicates that band 5 is consistent with AMR.

B. Bands 10 and 11

The experimental angular momentum of the $\Delta I=1$ band 10 is shown in Fig. 6 in comparison with the TAC calculation for the configuration $\pi[(g_{9/2})^{-2}]_{8^+}\otimes\nu[h_{11/2}]$ at the equilibrium deformation (at $\hbar\omega\approx 0.45$ MeV) $\varepsilon_2=0.10$, $\gamma=0°$. The backbend in this band was previously attributed to the first allowed $h_{11/2}$ neutron alignment (FG) [19], though the details of the alignment were not well understood—the presumed FG alignment was observed at a frequency lower than that predicted by the cranking model. This previous study involved calculations using a PAC approach; the additional degree of freedom introduced by the tilting angle θ, however, allows the first alignment for the positive-parity neutrons of mixed $g_{7/2}/d_{5/2}$ character (AB alignment) to move lower in rotational frequency as the cranking axis moves away from the principal-cranking axis of the nucleus. In fact, at the equilibrium value of θ determined in this calculation, the AB alignment precedes the FG alignment, and occurs at a frequency consistent with the experimentally observed alignment in this band. The upper part of band 10 is compared with the $\pi[(g_{9/2})^{-2}]_{8^+}\otimes\nu[h_{11/2}(g_{7/2}/d_{5/2})^2]$ configuration at the equilibrium deformation (at $\hbar\omega\approx 0.45$ MeV) of $\varepsilon_2=0.08$, $\gamma=12°$. Both parts of band 10 are in excellent agreement with their corresponding TAC calculations.

The newly observed transitions linking $\Delta I=1$ band 11 to states of known spin and parity suggest that the parity of band 11 is positive. The configuration of band 11 must, therefore, include either zero or two $h_{11/2}$ neutrons. Both the $\pi[(g_{9/2})^{-2}]_{8^+}\otimes\nu[(g_{7/2}/d_{5/2})]$ and $\pi[(g_{9/2})^{-2}]_{8^+}\otimes\nu[(g_{7/2}/d_{5/2})^3]$ configurations can be ruled out; the former is far too low in spin to be appropriate for band 11, and the latter is predicted to be less yrast than the configurations involving neutrons from the steeply downsloping $h_{11/2}$ orbitals. The most likely candidate is, hence, the $\pi[(g_{9/2})^{-2}]_{8^+}\otimes\nu[(g_{7/2}/d_{5/2})(h_{11/2})^2]$ configuration, which agrees with the tentative assignment proposed in Ref. [19]. This configuration assignment is supported by the observation that band 11 predominantly feeds two structures that were shown in Ref. [19] to most likely have the configurations $\pi[(g_{9/2})^{-2}]_{8^+}\otimes\nu[(g_{7/2}/d_{5/2})]$ (band 14) and $\pi[(g_{9/2})^{-2}]_{0^+}\otimes\nu[(g_{7/2}/d_{5/2})(h_{11/2})^2]$ (band 3). The experimental angular momentum I of band 11 is also shown in Fig. 6 in comparison with the TAC calculation for this configuration at the equilibrium deformation (at $\hbar\omega\approx 0.40$ MeV) of $\varepsilon_2=0.11$, $\gamma=10°$. The TAC calculations reasonably reproduce the general behavior of band 11. The upbend in this band is attributed to the positive-parity BC neutron alignment, predicted by the TAC codes to be the next allowed alignment. The difference in the sharpness of the alignment (see Fig. 6) may be due to improper treatment by the TAC codes of the interaction strength at the BC alignment. The sharpness of a crossing is a sensitive function of the chemical potential λ_ν. Imprecision in the value of λ_ν used in the TAC calculations may lead to too sharp a crossing due to uncertainties in the positions of single-particle levels. In addition, the calculations used the same value for the pairing constant Δ_ν throughout the entire range of rotational frequencies. Experimentally, one would expect Δ_ν to decrease in value at high frequencies, resulting in a less sharp alignment than that shown in the calculation in Fig. 6. This may also account for the larger disagreement found for the high-frequency states in this band.

The weighted average $B(M1)$ values extracted from the lifetime fits for bands 10 and 11 are shown in Fig. 7 in comparison with theoretical predictions from the TAC codes. Two TAC curves are shown for each band, corresponding to the effective intrinsic g factors $g_{s,eff}=fg_s$, where the spin attenuation factor f is 0.7 or 0.5. The value $f=0.7$ has been used consistently for the TAC calculations in the $Z=50$ region, though a value for f of 0.6 or lower seems more appropriate for reproducing the experimentally observed g factors for particles in this region [29]. The appropriate $B(M1)$ curves are, therefore, expected to fall between the two extremes shown on the plot.

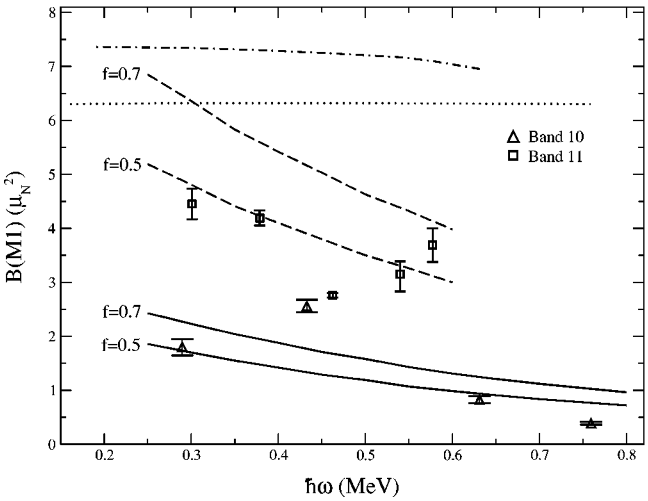

FIG. 7. Reduced $M1$ transition strength $B(M1)$ as a function of frequency for bands 10 and 11. Experimental values are the weighted averages of all three angle sets, deduced from the fitted lifetimes (see Table I). Two TAC curves are shown for both configurations, corresponding to a spin attenuation factor $f=0.7$ or 0.5. $B(M1)$ values deduced using the standard Dönau-Frauendorf fixed-K formalism are also shown for comparison; the dotted curve corresponds to the configuration for band 10 and the dash-dotted curve is for band 11. Both Dönau-Frauendorf curves were deduced assuming pure $g_{7/2}$ character for the positive-parity neutrons (see text).

The overall trend of the data points for band 10 is that of a curve that decreases with increasing frequency (or spin), characteristic of a shears band. The measured value for the 433-keV transition, however, is noticeably higher than the others in the band. There is no evidence of any contaminant peaks or other problems with the fitting procedure that could account for this discrepancy. There are, however, a number of $I^\pi=\frac{35}{2}^-$ states with similar excitation energies: (tentatively) the state at 5951 keV feeding into band 10, the 5969-keV state in band 5, the 6160-keV state in band 10, and (tentatively) the 6238-keV state in band 15. The proximity of these states may result in admixed wave functions which could account for the perturbation of the $B(M1)$ of the 433-keV transition. [As pointed out earlier, the 920-keV transition feeding out of the $\frac{35}{2}^-$ level of band 5 has a perturbed $B(E2)$ as well.] The TAC calculation reproduces the decreasing trend and the approximate magnitude of the band 10 data.

The $B(M1)$ values for band 11 behave similarly to band 10; apart from the point for the 577-keV transition, the $B(M1)$ values exhibit the characteristic decreasing trend as a function of frequency and are reasonably well reproduced by the TAC predictions. There is a contaminant peak at 577 keV in band 14 that is present in the gate for the 577-keV γ ray in band 11, but the LINESHAPE code allows for the proper inclusion and fitting of contaminant peaks, making it unlikely that the presence of the second peak is the cause for the perturbed $B(M1)$ value. For this case, it was noted that the errant point falls at about the spin where the BC alignment begins (see Fig. 6). The alignment of a pair of nucleons may result in the formation of new shears blades with a larger $B(M1)$ strength. Experimentally, one would expect to observe $B(M1)$ values which decrease with increasing spin for the states below an alignment, increase at the alignment, and then fall off again with increasing spin for states above the alignment. The increase in $B(M1)$ strength for the 577-keV transition in band 11 may reflect this behavior, though unfortunately lifetimes could not be measured high enough in the band to observe the $B(M1)$ behavior above the backbend.

Calculations were also performed for both bands using the semiclassical (fixed-K) formalism of Dönau and Frauendorf [10] to contrast with the TAC predictions. As can be seen in Fig. 7, these curves are nearly constant as a function of frequency (spin) and are significantly offset from the magnitude of the measured $B(M1)$ strengths. The positive-parity neutrons were assumed to be of pure $g_{7/2}$ character for the purpose of these calculations. (TAC calculations with $\theta \approx 90°$ indicate that this is a reasonable approximation.) Inclusion of a $d_{5/2}$ admixture results in curves which are $\sim 20\%$ lower in magnitude for band 10, which includes two active positive-parity neutrons, and $\sim 5\%$ lower for band 11, which includes one, but are still unable to reproduce the magnitude or slope of the data. This reasonably demonstrates that angular momentum in these observed bands cannot be generated by maintaining a fixed-K projection and cranking around a principal axis of the nucleus, but must involve a mechanism by which $\mu_{\perp}$ becomes smaller with increasing spin, as predicted by the TAC theory.

C. Semiclassical shears formalism

In addition to the TAC analysis discussed above, an analysis was performed for the $\Delta I = 1$ bands using the formalism presented in Refs. [17,30,31] as a semiclassical interpretation of the shears mechanism. Reference [31] discusses a means of estimating the core contribution to the angular momentum for a shears band. The core component is assumed to be a linear function of spin, i.e., $R_{core} = (\Delta R/\Delta I)(I - I_b)$, where ΔR is the difference between the maximum observed spin and the maximum spin that can be generated from the fully closed blades of the shears $(I_{max} - [j_\pi + j_\nu])$, ΔI is the range of observed spins in the band $(I_{max} - I_b)$, and I_b is the bandhead spin. For each configuration, j_π was taken to be 8 and j_ν was chosen such as to approximately reproduce the spin of the lowest observed state (assumed to be the bandhead) when the blades are perpendicular. For band 10 below the backbend, a small ($< 10\%$) core contribution is estimated using this approach. For the cases of band 10 above the backbend and band 11, the maximum observed spin for each configuration is equal to the maximum that can be generated by the closing shears blades, so the core contribution is negligible ($\mathbf{R} \approx 0$). This approach, however, assumes that the configurations in question have been observed to their terminating states. This is not necessarily the case here, where the configurations being considered may have been crossed by more yrast configurations prior to termination. In such an event, this model would underestimate the core contribution. The TAC calculations, on the other hand, explicitly include core effects. According to the TAC calculations, the fraction of the total spin attributable to core rotation was 0.38, 0.04, and 0.32 for band 10 below and above the alignment and band 11, respectively; these values are significantly larger than the corresponding estimates given above for the bottom part of band 10 and for band 11. This would suggest that the configurations are not, in fact, seen to termination, and that caution should be used when applying the method outlined in Ref. [31] to estimate the core contribution. It is apparent from both models, however, that the shears is the dominant contribution to the total angular momentum.

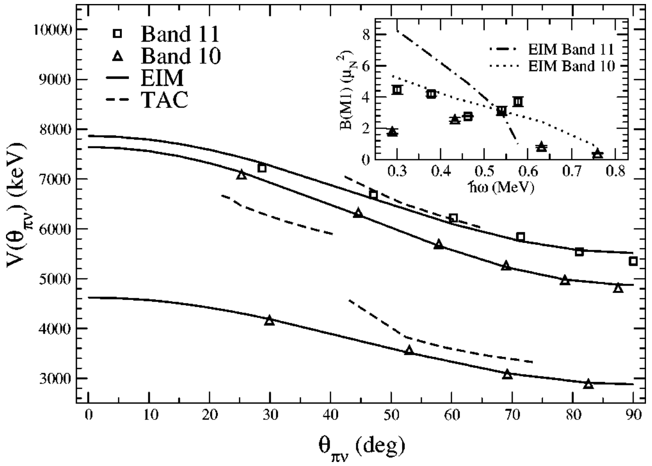

FIG. 8. Excitation energy as a function of shears angle $\theta_{\pi\nu}$. Experimental energies are relative to the $\frac{11}{2}^-$ state in band 5. Solid curves are the results of fits to the data with a function of the form $V_2 P_2(\cos\theta_{\pi\nu}) + V_0$ for the effective-interaction model (EIM). Dashed lines are values extracted from the TAC calculations. Note that only the relative energies of the three configurations are determined by the TAC codes; the absolute energy scale has been adjusted for comparison with the data. The inset shows a plot of the corresponding $B(M1)$ versus frequency deduced using EIM.

Reference [30] proposed that the shears mechanism is generated by a residual interaction between the proton and neutron blades with a strength proportional to $P_2(\cos\theta_{\pi\nu})$, where $\theta_{\pi\nu}$ is the angle between the blades (shears angle). Experimentally, the shears angle for a pure shears band ($\mathbf{R} = 0$) can be estimated at each observed spin I by calculating $\theta_{\pi\nu} = \cos^{-1}[(I^2 - j_\pi^2 - j_\nu^2)/2 j_\pi j_\nu]$. The excitation energy of each state for pure shears should result solely from the closing of the blades. As discussed above, bands 10 and 11 are not pure shears bands, but because of its small core contribution, the top part of band 10 can be approximated by a pure shears. For comparative purposes and to simplify the remainder of this analysis using the effective-interaction model (EIM), each band was treated as if $\mathbf{R} \equiv 0$; the ramifications of this assumption will be addressed.

The energies of states in each band relative to the $\frac{11}{2}^-$ state of band 5 were calculated and are plotted as a function of $\theta_{\pi\nu}$ in Fig. 8; these results are fitted with a function of the form $V(\theta_{\pi\nu}) = \frac{1}{2} V_2 (3\cos^2\theta_{\pi\nu} - 1) + V_0$, which is appropriate for a force generated by the exchange of a quadrupole phonon. A good fit to this function is observed for band 10, both below and above the alignment; band 11 deviates somewhat from this form, but is still reasonably well reproduced. The strength of the interaction is determined by the value of V_2 for each sequence. The fits yield $V_2 \sim 1200$, 1800, and

1600 keV for the bottom and top of band 10 and band 11, respectively. The corresponding number of proton-hole/neutron pairs is 2×1 for the lower part of band 10 and 2×3 for the upper part of band 10 and for band 11, resulting in an interaction strength per proton-hole/neutron pair of ~ 600, 300, and 250 keV/pair. In a similar analysis [4], a strength of ~ 500 keV/pair was estimated for ^{110}Cd and compared with ~ 300 keV/pair for ^{198}Pb. The bands discussed in this paper do not appear to be consistent with the $1/A$ dependence of the interaction strength suggested in [30].

In addition to the assumption that $\mathbf{R}=0$, this semiclassical analysis is further complicated by the assumption that there are two rigid shears blades, one for proton holes and one for neutrons. For the upper states of band 10 and for band 11, this assumption is not valid due to the presence of the $(g_{7/2}/d_{5/2})$ neutrons. While the $g_{9/2}$ proton holes have a high-Ω projection and the $h_{11/2}$ neutrons have a low-Ω projection, the positive-parity neutrons are mid-Ω, oriented roughly in the direction of the tilted cranking axis, essentially forming a third blade. The previous analysis was repeated for the top of band 10 and for band 11, but with the spin of each state I replaced with $I'=I-\Sigma j_{\nu(g_{7/2}/d_{5/2})}$. (The lower part of band 10 does not involve active positive-parity neutrons.) The residual interaction was then treated as if acting only between the proton-hole and $h_{11/2}$-neutron blades. Fits to the corresponding $V(\theta_{\pi\nu})$ values resulted in interaction strengths of ~ 650 and 450 keV/pair for bands 10 and 11, respectively, which is more consistent with the results for the bottom of band 10 and for the band in ^{110}Cd. [Although agreement with the latter is perhaps surprising since the band in ^{110}Cd includes $(g_{7/2}/d_{5/2})$ neutrons as well and should suffer the same complication as the bands in ^{109}Cd.]

It is apparent from Fig. 8 that reasonable fits are achievable despite the somewhat inappropriate assumption that $\mathbf{R}=0$. Careful consideration of the core is needed to avoid misleading results. If the core was included in the fits for the lower part of band 10 and for band 11, part of the total angular momentum would be generated by the core. The blades of the shears would close more slowly, resulting in a smaller range of shears angles for the observed states in each band. The excitation energy of each state, however, would also be partly due to the core as well as the shears. Without a more detailed analysis, the effect the inclusion of the core has on the shape of the curves is not transparent. The upper part of band 10, however, having a minimal core component, should make a reasonably good example of the usage of this model.

To compare the two shears models considered in this work, the shears angle and corresponding excitation energies were also extracted from the TAC calculations and plotted in Fig. 8 (dashed curves). The shears angle was taken to be the angle between the proton-hole blade and the blade formed by the sum of all valence neutrons, for comparative purposes. One point that becomes immediately apparent is that the range of shears angles for a given configuration is significantly smaller for the TAC predictions than for the EIM predictions. For the lower part of band 10 and for band 11, this large difference is not surprising; without a core component in the EIM calculations, the shears blades must close faster to generate angular momentum. The upper part of band 10, however, was shown in both models to have a negligible core component, yet this large difference in the range of angles persists. The rapid close of the shears in the EIM calculations implies a rapid decrease in the magnitude of the $\mu_{\perp}$ vector, and hence a dramatic decrease in $B(M1)$ strength is expected. This behavior is demonstrated in the inset to Fig. 8; the $B(M1)$ values were calculated using the expression in [30], with g_{ν} determined by assuming that all the $\mathbf{j}_{\nu}$ vectors were parallel, i.e., $g_{\nu}=(1/\Sigma j_{\nu_i})(\Sigma g_{\nu_i} j_{\nu_i})$. [The $B(M1)$ strengths were also evaluated assuming the positive-parity neutrons were aligned parallel to the cranking axis and hence contributed nothing to the $B(M1)$; the results did not differ much from those shown in the figure.] It is clear from this plot that the EIM calculations do not properly reproduce the measured transition probabilities, even for the states in band 10 which are expected to have negligible core effects.

This effective-interaction model may be a useful model for interpreting shears bands from a phenomenological perspective, and has been successfully applied to the Pb region [17,30,31], where the shears bands consist of long, rigid high- and low-K blades in nuclei with small deformations. The model involves some simplifying assumptions, however, which may limit its applicability to certain cases, as demonstrated in the current analysis.

V. CONCLUSIONS

In summary, lifetimes of states in two $\Delta I=1$ bands and one $\Delta I=2$ band in ^{109}Cd have been measured using the Doppler shift attenuation method in an experiment performed with the GAMMASPHERE array. The deduced $B(M1)$ values for the dipole bands exhibit the characteristic decrease as a function of spin expected for the shears mechanism. This decrease cannot be explained in the context of the traditional formalism whereby K remains fixed and angular momentum is generated by collective rotation about an axis perpendicular to the symmetry axis of the nucleus. Angular momentum and $B(M1)$ values were calculated using tilted axis cranking codes, and have been shown to be consistent with the experimental results. The angular momentum and $B(E2)$ values deduced for the $\Delta I=2$ band have also been shown to be consistent with principal axis cranking calculations for an antimagnetic rotor. The ratio $\mathcal{J}^{(2)}/B(E2)$ was found to be an order of magnitude larger for this band than for well-deformed rotors, indicating a large contribution to the moment of inertia from the closing shears blades. An alternate model for the shears mechanism involving proton-neutron effective interactions where the strength is proportional to $P_2(\cos\theta_{\pi\nu})$ was also applied to the $\Delta I=1$ bands. An interaction strength of ~ 600 keV/pair was estimated using this model, though limitations of the applicability of this model exist. Both models predict that the majority of the angular momentum in each band is generated by the alignment of proton-hole and neutron blades, consistent with the suggestion, based on analyses of Pb isotopes, that the shears mechanism should dominate in nuclei with $\varepsilon_2 \lesssim 0.12$.

ACKNOWLEDGMENTS

The authors would like to thank J. Wells for providing the LINESHAPE codes and assistance in getting them running at Stony Brook, the staff of the 88-Inch Cyclotron for providing the beam, and K. Starosta and D. R. LaFosse for many helpful discussions. This work was supported in part by the NSF under Grant No. 431-0980H, the DOE under Contract Nos. DE-AC03-76SF00098 and DE-FG02-95-ER40934, and the UK EPSRC.

---

[1] A. Kuhnert *et al.*, Phys. Rev. C **46**, 133 (1992).
[2] R. M. Clark *et al.*, Nucl. Phys. **A562**, 121 (1993).
[3] G. Baldsiefen *et al.*, Nucl. Phys. **A592**, 365 (1995), and references therein.
[4] R. M. Clark *et al.*, Phys. Rev. Lett. **82**, 3220 (1999).
[5] A. Gadea *et al.*, Phys. Rev. C **55**, R1 (1997).
[6] D. G. Jenkins *et al.*, Phys. Lett. B **428**, 23 (1998).
[7] D. G. Jenkins *et al.*, Phys. Rev. C **58**, 2703 (1998).
[8] S. Frauendorf, Nucl. Phys. **A557**, 259c (1993).
[9] S. Frauendorf, Rev. Mod. Phys. (to be published).
[10] F. Dönau and S. Frauendorf, in *Proceedings of the International Conference on High Angular Momentum Properties of Nuclei, Oak Ridge, 1982*, edited by N. R. Johnson (Harwood, New York, 1983), p. 143.
[11] R. M. Clark *et al.*, Phys. Rev. Lett. **78**, 1868 (1997).
[12] R. M. Clark *et al.*, Phys. Lett. B **440**, 251 (1998).
[13] R. Krücken *et al.*, Phys. Rev. C **58**, R1876 (1998).
[14] N. S. Kelsall *et al.* Phys. Rev. C **61**, 011301(R) (2000).
[15] D. G. Jenkins *et al.*, Phys. Rev. Lett. **83**, 500 (1999).
[16] S. Frauendorf, Z. Phys. A **358**, 163 (1997).
[17] A. O. Macchiavelli, R. M. Clark, M. A. Deleplanque, R. M. Diamond, P. Fallon, I. Y. Lee, F. S. Stephens, and K. Vetter, Phys. Lett. B **450**, 1 (1999).
[18] S. Frauendorf, in *Proceedings of the Workshop on Gammasphere Physics, Berkeley, 1995*, edited by M. A. Deleplanque, I. Y. Lee, and A. O. Macchiavelli (World Scientific, Singapore, 1996).
[19] S. Juutinen *et al.*, Nucl. Phys. **A577**, 727 (1994).
[20] J. Gascon *et al.*, Nucl. Phys. **A513**, 344 (1990), and references therein.
[21] P. J. Nolan, F. A. Beck, and D. B. Fossan, Annu. Rev. Nucl. Part. Sci. **44**, 561 (1994).
[22] D. C. Radford, Nucl. Instrum. Methods Phys. Res. A **361**, 297 (1995).
[23] S. Juutinen *et al.* (unpublished).
[24] J. C. Wells and N. Johnson (private communication).
[25] L. C. Northcliffe and R. F. Schilling, Nucl. Data, Sect. A **7**, 233 (1970).
[26] F. James and M. Roos, Comput. Phys. Commun. **10**, 343 (1975).
[27] H. Ejiri and M. J. A. de Voigt, *Gamma Ray and Electron Spectroscopy in Nuclear Physics* (Oxford University Press, Oxford, England, 1987), p. 504.
[28] M. Piiparinen *et al.* (unpublished).
[29] T. Lonnröth, S. Vajda, O. C. Kistner, and M. H. Rafailovich, Z. Phys. A **317**, 215 (1984).
[30] A. O. Macchiavelli, R. M. Clark, P. Fallon, M. A. Deleplanque, R. M. Diamond, R. Krücken, I. Y. Lee, F. S. Stephens, S. Asztalos, and K. Vetter, Phys. Rev. C **57**, R1073 (1998).
[31] A. O. Macchiavelli, R. M. Clark, M. A. Deleplanque, R. M. Diamond, P. Fallon, I. Y. Lee, F. S. Stephens, and K. Vetter, Phys. Rev. C **58**, R621 (1998).